

Anisotropic superconductivity mediated by ferroelectric fluctuations in cubic systems with spin-orbit coupling

Maria N. Gastiasoro,^{1,*} Thaís V. Trevisan,^{2,†} and Rafael M. Fernandes¹

¹*School of Physics and Astronomy, University of Minnesota, Minneapolis 55455, USA*

²*Instituto de Física Gleb Wataghin, Unicamp, Rua Sérgio Buarque de Holanda, 777, CEP 13083-859 Campinas, SP, Brazil*

(Dated: February 1, 2022)

Motivated by the experimental observation that superconductivity in bulk doped SrTiO₃ is enhanced as a putative ferroelectric quantum critical point (FE-QCP) is approached, we study the pairing instability of a cubic system in which electrons exchange low-energy ferroelectric fluctuations. Instead of the gradient coupling to the lattice distortion associated with ferroelectricity, we consider a direct coupling between the electrons and the bosonic ferroelectric field that appears in the presence of spin-orbit coupling. Working in the weak-coupling regime, we find that the pairing interaction is dominated by the soft transverse optical (TO) mode, resulting in a T_c enhancement upon approaching the FE-QCP. Focusing on even-parity states, we find that although the s -wave state always wins, states with higher Cooper-pair angular momentum become close competitors as the TO mode softens. We show that the cubic anisotropy of the FE fluctuations mixes the s -wave and g -wave states, resulting in a characteristic anisotropy of the gap function. The gap anisotropy behaves non-monotonically as the FE-QCP is approached: upon decreasing the TO mode frequency, the gap anisotropy first changes sign and then increases in magnitude. We discuss the possible applications of our results to the superconducting state of SrTiO₃.

I. INTRODUCTION

The possibility that bosonic excitations other than phonons can promote superconductivity has a long history. The fact that the pairing state of high- T_c cuprates is observed in close proximity to an antiferromagnetic state has encouraged intense theoretical investigations about the nature of the superconducting state mediated by antiferromagnetic fluctuations [1–6]. Beyond cuprates, the phase diagrams of certain heavy fermions and iron pnictides have motivated theoretical studies of pairing promoted by the exchange of ferromagnetic fluctuations [7] and nematic fluctuations [8, 9]. More recently, the idea that ferroelectric fluctuations can also mediate the formation of Cooper pairs [10, 11] has spurred considerable interest, particularly in the context of doped bulk SrTiO₃ (STO) – for a recent review, see Ref. [12]. Indeed, undoped STO is a semiconducting quantum paraelectric, i.e. a material whose quantum fluctuations prevent the onset of the classical ferroelectric ground state [13, 14]. Upon doping via oxygen vacancies or niobium substitution, a superconducting dome emerges already at very small carrier concentrations [15–17]. By tuning doped (i.e. metallic) STO towards a ferroelectric transition, which can be accomplished via isotope oxygen substitution [18], chemical substitution on the cation site [19, 20], hydrostatic pressure [21] or strain [22, 23], it is generally observed that the superconducting transition temperature T_c increases as the putative zero-temperature ferroelectric transition is approached. This is particularly unexpected in the case of ¹⁸O substituted STO [18, 20], since the standard isotope effect would predict a lower T_c due to the fact that ¹⁸O is heavier than ¹⁶O.

It is important to emphasize that a metal cannot sus-

tain macroscopic ferroelectricity due to screening effects. But in STO, the displacive ferroelectric transition is accompanied by a structural transition in which the crystal changes from centrosymmetric to non-centrosymmetric. As a result, the ferroelectric transition is signaled not only by a diverging dielectric constant [13, 14, 24], but also by an accompanying softening of a transverse optical (TO) phonon mode [25–27]. Strain fluctuations associated with the TO mode persist even in the metallic phase, and thus can mediate electron-electron interactions even if there are no macroscopic dipole moments. Because locally the electric polarization is proportional to the lattice displacement, we will refer to the pairing mechanism as promoted by ferroelectric fluctuations, and to the ordered state as a metallic ferroelectric state [28, 29].

Different theoretical models have been proposed to study the scenario in which pairing is due to the exchange of such ferroelectric fluctuations. Edge *et al.* considered an effective model in which the zero-temperature (i.e. quantum) ferroelectric phase transition in STO is described in terms of a transverse field Ising model, which couples directly via a Yukawa-type coupling to the electronic density [10]. They obtained a superconducting dome as the carrier concentration increases due to the competition between the enhancement of the density of states and the suppression of the soft TO mode upon doping. They also predicted the aforementioned unusual isotope effect in ¹⁸O substituted STO. One problem however is how the TO mode microscopically couples to the electronic degrees of freedom. Because the TO mode is polar, the standard electron-phonon matrix element gives a gradient coupling between the lattice displacement and the electronic density. As a result, the soft TO mode effectively decouples from the electronic states, and the

main contribution to the pairing interaction comes from the associated longitudinal optical (LO) mode, which remains massive even at the ferroelectric transition. Wölfle and Balatsky pointed out that the cubic anisotropy of the lattice allows for an effective coupling between the TO mode and the electronic density away from high-symmetry directions [30]. However, such a coupling was later argued to be too small [31].

An alternative coupling between the odd-parity TO mode and the electrons occurs when spin-orbit coupling (SOC) is present [32]. This allows for a direct coupling between the fermions and the bosonic fields that avoids the gradient coupling discussed above. Kozii and Fu recently studied how superconductivity emerges in the general case of electrons spin-orbit-coupled to a generic bosonic mode that breaks inversion symmetry [33]. They found the interesting possibility of closely competing even-parity and odd-parity pairing states. Kanasugi and Yanase considered the same coupling to study the interplay between superconductivity and long-range ferroelectric order in STO [34, 35]. However, in their model, the pairing interaction did not arise directly from the ferroelectric fluctuations, i.e. long-range superconducting and ferroelectric orders were treated as separate states.

Motivated by these previous investigations, in this paper we solve the weak-coupling problem in which pairing is mediated by the exchange of an inversion-symmetry-breaking vectorial bosonic field that couples to the electrons via the SOC, as relevant for bulk STO. We explicitly take into account the role of the cubic crystal-field anisotropy present in these systems, an effect that has been largely unexplored in previous works. We find that, in the singlet channel, the *s*-wave pairing channel dominates, and the pairing interaction is strongly enhanced as the ferroelectric transition is approached. Moreover, the subleading larger angular momentum pseudospin-singlet channels (*d*-wave and *g*-wave) become gradually more competitive as the TO mode becomes softer and the putative ferroelectric quantum critical point (FE-QCP) is approached. Interestingly, the lattice cubic anisotropy leads to an anisotropy of the gap function. Although the anisotropy that we find is never large enough to induce accidental nodes, it increases in magnitude and changes its sign as the frequency of the TO mode decreases. As a result, the gap maxima and gap minima switch locations around the Fermi surface as the FE-QCP is approached.

We emphasize that the pairing solution studied here is in the weak-coupling (i.e. BCS-like) limit, since the dynamics of the bosons are not taken into account. This approximation is of course not valid close enough to the FE-QCP, where the feedback effect of the fermions on the boson dynamics is expected to play a crucial role. Moreover, in our approach, because the main contribution to the pairing interaction comes from the soft TO mode, whose energy is smaller than the Fermi energy, the impact of the LO mode, whose energy is larger than the

Fermi energy, is negligible. Of course, the LO mode on its own can mediate pairing, as discussed elsewhere [36]. Despite these approximations, our work reveals a clear qualitative evolution of the gap function as the FE-QCP is approached. We thus discuss the possible implications of our results to the elucidation of superconductivity in STO, highlighting the issues that remain to be addressed to confirm whether this scenario is suitable.

The paper is organized as follows: in Sec. II we introduce the model, which includes a spin-orbit mediated direct coupling between the low-energy fermions and the FE fluctuations, and obtain the effective pairing interaction and superconducting gap equation. We first solve for T_c assuming rotational invariance in Sec. III, and investigate the close competition among even-parity channels as the TO mode softens. In Sec. IV we include the finite cubic crystal-field in the FE fluctuations and study the resulting anisotropy of the gap function. We show a characteristic sign change and subsequent growth of this anisotropy as the FE instability is approached. We summarize our results and discuss the possible applications to superconductivity in STO in Sec. V. Appendices A and B expand on technical details of the main calculations.

II. LOW-ENERGY MODEL

Our model consists of non-interacting fermions $c_{\mathbf{k}\alpha}$, with momentum \mathbf{k} and (pseudo-)spin projection α , coupled to ferroelectric (FE) excitations in a cubic lattice described by the vector bosonic field $\phi(\mathbf{q})$. The latter is parity-odd and time-reversal-even; as a result, it is proportional to the polar lattice displacement \mathbf{u} that promotes a local polarization $\mathbf{P} \propto \mathbf{u}$ inside the cubic unit cell. Since we are working in the metallic regime, the system does not sustain a macroscopic polarization. Yet, as we discussed above, we refer to $\phi(\mathbf{q})$ as the FE order parameter or polarization. Similarly, we refer to the FE mode and the TO phonon mode interchangeably.

A. Bosonic propagator: optical phonons

The bosonic propagator describing the FE fluctuations in the disordered state is given by [12, 30, 31, 37, 38]

$$\chi_{ij}^{-1}(\mathbf{q}, i\Omega_n) = E_T^{-1} [K_i(\mathbf{q})\delta_{ij} + M(q)\hat{q}_i\hat{q}_j] , \quad (1)$$

with Matsubara bosonic frequency $\Omega_n = 2n\pi T$ ($n \in \mathbb{Z}$) and:

$$K_i(\mathbf{q}) = \Omega_n^2 + \omega_T^2 + E_T^2 q^2 + \varepsilon_c^2 q_i^2 , \quad (2)$$

$$M(q) = \omega_L^2 - \omega_T^2 - (E_T^2 - E_L^2) q^2 . \quad (3)$$

Here, the Latin indices i, j refer to components of the FE order parameter ϕ_i . The eigenvalues of Eq.(1) give the phonon dispersions of two transverse optical (TO)

modes and one longitudinal optical (LO) mode, which have the characteristic energy scales $E_T \equiv c_T \pi/a$ and $E_L \equiv c_L \pi/a$, respectively, with a denoting the cubic lattice constant. The quantities c_T (c_L) and ω_T (ω_L) denote the transverse (longitudinal) phonon velocity and the transverse (longitudinal) optical gap at the center of the Brillouin zone, respectively. Importantly, $\omega_L^2 = \omega_T^2 + \omega_p^2$, where ω_p is the ionic plasma frequency; this term arises because the LO mode generates Coulomb energy. Thus, ω_L remains finite even when $\omega_T \rightarrow 0$ at the FE transition. Note that our choice of units is such that the propagator has dimensions of inverse of energy, and the transferred momentum \mathbf{q} has units of π/a in Eqs.(1)-(3).

A crucial parameter in Eq. (3) is the cubic anisotropy term ε_c , which arises from the crystal field effects of the cubic lattice. If it is absent ($\varepsilon_c = 0$), the phonon propagator is rotationally invariant and can be rewritten in the form:

$$\frac{\chi_{ij}^{-1}(\mathbf{q}, i\Omega_n)}{E_T^{-1}} = \Omega_n^2 \delta_{ij} + (\omega_L^2 + E_L^2 q^2) \hat{q}_i \hat{q}_j \quad (4)$$

$$+ (\omega_T^2 + E_T^2 q^2) (\delta_{ij} - \hat{q}_i \hat{q}_j)$$

As a result, the eigenvalues split into a doubly-degenerate purely transverse mode, $\varpi_T^2(\mathbf{q}) = \omega_T^2 + E_T^2 q^2$, and a purely longitudinal mode, $\varpi_L^2(\mathbf{q}) = \omega_L^2 + E_L^2 q^2$. A non-zero ε_c , on the other hand, breaks rotational symmetry and mixes the longitudinal and transverse polarization of the modes, except along high-symmetry directions [30, 31]. The dispersions themselves become anisotropic, as shown in Fig. 1, which contrasts the three isotropic modes for $\varepsilon_c = 0$ (panels (a) to (c)) to the three anisotropic modes for $\varepsilon_c \neq 0$ (panels (d) to (f)). As we explain later, the cubic anisotropy has an important impact on the gap function in the superconducting state. In this figure and in the remainder of the text, we set the following parameters: $\omega_L = 100$ meV, $E_T = 40$ meV, and $E_L = E_T/10$, which fit well the neutron scattering data of Ref. [27].

B. Coupling to electronic degrees of freedom

We now consider how the FE fluctuations discussed above couple to the electronic degrees of freedom. For simplicity, we will restrict our analysis to a single-band with dispersion $\xi_{\mathbf{k}} = k^2/2m - \mu$, where μ is the chemical potential, as appropriate for dilute STO. The most straightforward coupling between the FE bosonic field ϕ and the fermions $c_{\mathbf{k}\alpha}$ is via the standard electron-phonon coupling. Due to the dipolar nature of the phonons, this translates into a gradient coupling [30, 39, 40]. As a result, there is no direct coupling between the modes with transverse polarization and the electronic density. In the case where the cubic anisotropy term vanishes, $\varepsilon_c = 0$,

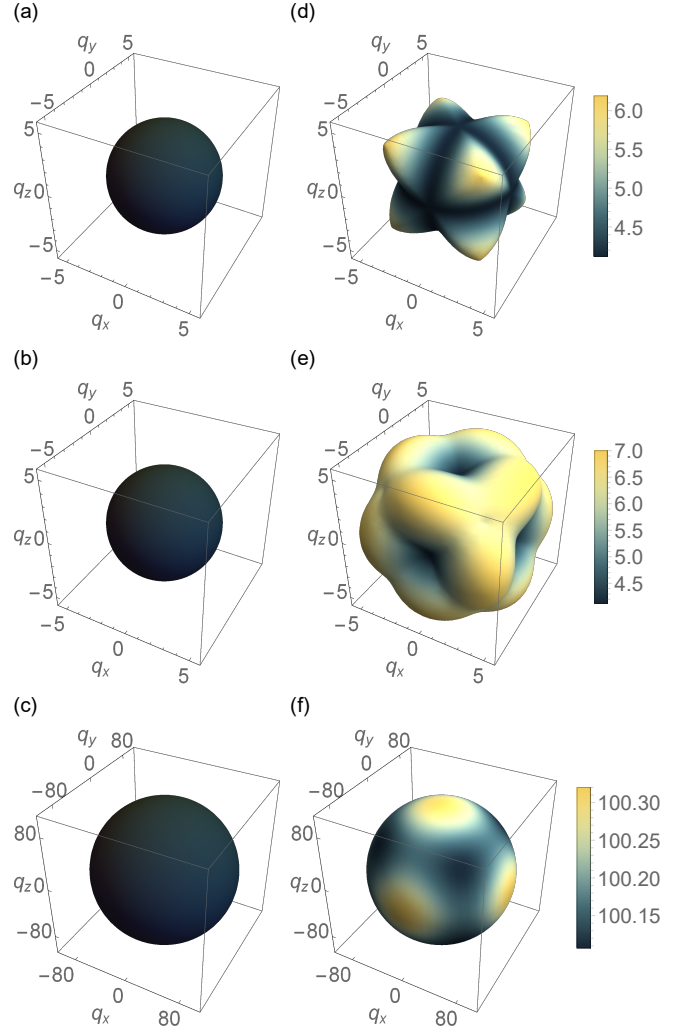


Figure 1. Dispersions of the phonon propagator Eq. (1) at finite $q = 0.1$ without a crystal field $\varepsilon_c = 0$ in panels (a)-(c) and with a finite cubic crystal field $\varepsilon_c = 2E_T$ in panels (d)-(f). (a) and (b) are the purely transverse modes $\varpi_T(q)$ and (c) is the purely longitudinal mode $\varpi_L(q)$. The eigenmodes of the dispersions (d)-(f) are anisotropic; their polarizations are neither purely longitudinal nor purely transverse except at high-symmetry directions of the cubic crystal. In all panels $\omega_T = 1$ meV, $\omega_L = 100$ meV, $E_T = 40$ meV, and $E_L = E_T/10$.

this would imply a complete decoupling from the soft TO mode. The presence of $\varepsilon_c \neq 0$, however, mixes transverse and longitudinal polarizations (except along high-symmetry directions), allowing for an indirect coupling to the TO mode [30]. Such a coupling, however, is expected to be very small, particularly in the dilute regime of STO [31].

In this work, we consider instead another allowed coupling, which is present in systems with spin-orbit coupling (SOC), as previously discussed in Refs. [32, 33, 41, 42]. The Hamiltonian in this case is given by

$$\hat{H} = \sum_{\mathbf{k}, \alpha} \xi_{\mathbf{k}} c_{\mathbf{k}\alpha}^\dagger c_{\mathbf{k}\alpha} + g \sum_{\mathbf{q}} \sum_i \phi_i(\mathbf{q}) \hat{Q}_i(\mathbf{q}). \quad (5)$$

where g is a coupling constant with dimensions of energy. Following the notation of Refs. [33, 41], the bilinear electronic operator that couples directly to the parity-odd bosonic field can be written as:

$$\hat{Q}_i(\mathbf{q}) \equiv \sum_{\mathbf{k}, \alpha\beta} F_{i,\alpha\beta}(\mathbf{k}, \mathbf{q}) c_{\mathbf{k}+\mathbf{q}, \alpha}^\dagger c_{\mathbf{k}\beta}, \quad (6)$$

where the form factor is:

$$F_{i,\alpha\beta}(\mathbf{k}, \mathbf{q}) = \frac{1}{2} [\Gamma_{i,\alpha\beta}(\mathbf{k} + \mathbf{q}) + \Gamma_{i,\alpha\beta}(\mathbf{k})], \quad (7)$$

$$\Gamma_{i,\alpha\beta}(\mathbf{k}) = [\hat{k} \times \boldsymbol{\sigma}_{\alpha\beta}]_i, \quad (8)$$

Recall that the Latin indices i, j refer to the Cartesian components of the bosonic fields, whereas the Greek indices α, β refer to the pseudospin components of the fermionic field. Moreover, σ is a Pauli matrix. That such a term is allowed by symmetry follows from the fact that $\hat{Q}_i(\mathbf{q})$ is even under time-reversal but odd under inversion symmetry. The main question, of course, is about the magnitude of the coupling constant g , which remains unsettled in STO, to the best of our knowledge [43]. Qualitatively, such a coupling is fundamentally different than the gradient coupling mentioned above, since it allows for a finite coupling between the soft TO mode and the fermions even in the $\mathbf{q} \rightarrow 0$ limit. Quantitatively, it is expected that even if the coupling g is small, proximity to a FE-QCP moves the system towards the strong-coupling regime, since the pairing interaction becomes singular [2].

C. Superconducting gap equation

Our model consists of Eq. (5) supplemented by the bosonic propagator (1). To obtain the pairing instability, we employ the standard approach of computing the anomalous fermionic self-energy via the self-consistent rainbow diagram. To keep the calculation controlled, we will focus on the BCS (i.e. weak-coupling) regime. While this approximation does not give access to the behavior at the FE-QCP, it does provide important insight into the pairing problem as the QCP is approached, which is our goal in this paper. More specifically, as we show below, the pairing interaction goes approximately as g^2/ω_T^2 in this approximation. This defines a regime around the QCP where the soft-mode ω_T remains larger than g such that the pairing interaction remains in the weak-coupling regime. Thus, the smaller g is, the closer to the FE-QCP our approach is valid.

To proceed, we introduce the extended Nambu spinor $\hat{\psi}_{\mathbf{k}}^\dagger = (c_{\mathbf{k}\uparrow}^\dagger c_{\mathbf{k}\downarrow}^\dagger c_{-\mathbf{k}\uparrow} c_{-\mathbf{k}\downarrow})$ and rewrite the bare electronic



Figure 2. Diagrammatic representation of the dressed fermionic Green's function (double solid lines). The single solid lines correspond to the bare fermionic Green's function defined in Eq.(9), while the single dashed line represent the bare bosonic propagator defined in Eq.(1). The small dark circles denote the interaction vertex defined in Eq.(12).

Green's function,

$$\hat{\mathcal{G}}_0^{-1}(\mathbf{k}, \omega_n) = \frac{1}{2} (i\omega_n \sigma_0 \tau_0 - \xi_{\mathbf{k}} \sigma_0 \tau_3), \quad (9)$$

where $\omega_n = (2n+1)\pi T$ (with $n \in \mathbb{Z}$) is the fermionic Matsubara frequency and σ_j (τ_j) denotes the Pauli matrices in spin (particle-hole) space. Moreover, to shorten the notation we define $\hat{\mathcal{G}}_0(\mathbf{k}, \omega_n) \equiv \hat{\mathcal{G}}_{0,n}(\mathbf{k})$, $\chi_{ij}(\mathbf{q}, \Omega_n) \equiv \chi_{ij,n}(\mathbf{q})$, and similarly for all the other Green's functions and self-energies introduced in this section. The coupling between the electrons and the FE fluctuations dresses the bare electronic propagator according to Dyson's equation

$$\hat{\mathcal{G}}_n^{-1}(\mathbf{k}) = \hat{\mathcal{G}}_{0,n}^{-1}(\mathbf{k}) - \hat{\Sigma}_n(\mathbf{k}), \quad (10)$$

where the fermionic self-energy due to the summation of rainbow-type diagrams, illustrated in Fig. 2, takes the form

$$\hat{\Sigma}_n(\mathbf{k}) = 2T \sum_{\mathbf{k}', n', ij} \chi_{ij,n}(\mathbf{k} - \mathbf{k}') \hat{F}_j(\mathbf{k}, \mathbf{k}' - \mathbf{k}) \hat{\mathcal{G}}_{n'}(\mathbf{k}') \hat{F}_i(\mathbf{k}, \mathbf{k}' - \mathbf{k}). \quad (11)$$

Here, we defined $\hat{F}_i(\mathbf{k}, \mathbf{k}' - \mathbf{k}) \equiv g (\hat{\Gamma}(\mathbf{k}') + \hat{\Gamma}(\mathbf{k})) / 4$, where

$$\hat{\Gamma}(\mathbf{k}) = \begin{pmatrix} \Gamma_{\uparrow\uparrow}(\mathbf{k}) & \Gamma_{\uparrow\downarrow}(\mathbf{k}) & 0 & 0 \\ \Gamma_{\downarrow\uparrow}(\mathbf{k}) & \Gamma_{\downarrow\downarrow}(\mathbf{k}) & 0 & 0 \\ 0 & 0 & \Gamma_{\uparrow\uparrow}(\mathbf{k}) & \Gamma_{\downarrow\uparrow}(\mathbf{k}) \\ 0 & 0 & \Gamma_{\uparrow\downarrow}(\mathbf{k}) & \Gamma_{\downarrow\downarrow}(\mathbf{k}) \end{pmatrix} \quad (12)$$

denotes the matrix representation of Eq. (8) in Nambu space.

Note that, in the weak-coupling regime that we study in this paper, we can neglect the renormalization of the bosonic propagator Eq. (1) caused by the coupling to the electrons. Because of the structure of the form factor in Eq. (7), such a coupling is expected to give rise to a momentum-dependent Landau damping, which should affect the pairing problem at the FE-QCP, similarly to the case of a ferromagnetic QCP [7].

We solve the self-consistent equations (10) and (11) within the weak-coupling approximation, in which the dynamics of the bosonic propagator is neglected (i.e. $\chi_{ij}(\mathbf{k} - \mathbf{k}') \equiv \chi_{ij,0}(\mathbf{k} - \mathbf{k}')$) in lieu of a cut-off ω_c , and the states are assumed to be at the Fermi surface, i.e. $\mathbf{k} = k_F \hat{k}$. In addition, as relevant for STO, we focus

on the even-parity pseudospin-singlet channel, in which case the anomalous part of the self-energy is given by $\hat{\Sigma}_{\text{an}} = i\sigma_2\tau_1\Delta$. The resulting linearized gap-equation obtained from the self-consistent solution of Eq. (11) is given by

$$\Delta(\hat{k}) = \log\left(\frac{\kappa\omega_c}{T_c}\right) \int \frac{d\hat{k}'}{4\pi} \Delta(\hat{k}') \lambda(\hat{k}, \hat{k}') . \quad (13)$$

Here $\kappa = 2e^\gamma/\pi \approx 1.13$, and we defined the dimensionless pairing interaction function:

$$\lambda(\hat{k}, \hat{k}') = \frac{\lambda_0}{2} [L(\hat{k}, \hat{k}') + L(\hat{k}, -\hat{k}')] \quad (14)$$

Note that $\lambda(\hat{k}, \hat{k}')$ has been expressed explicitly as an even function of \hat{k}' , which is accomplished by using the fact that $\Delta(-\hat{k}') = \Delta(\hat{k}')$. In this expression, we defined the dimensionless electron-FE coupling constant $\lambda_0 = N_F g^2 E_T^{-1}$, where N_F is the density of states at the Fermi level. The solid angle dependence in the coupling function $L(\hat{k}, \hat{k}')$ causes the gap function $\Delta(\hat{k})$ to be generically anisotropic around the Fermi surface. This angular dependence is a result of both the form factor in Eq. (7) and the bosonic propagator Eq. (1):

$$L(\hat{k}, \hat{k}') = E_T \sum_{ij} f_{ij}(\hat{k}, \hat{k}') \chi_{ij}(\hat{k} - \hat{k}') \quad (15)$$

with:

$$f_{ij}(\hat{k}, \hat{k}') = [\Gamma_{i,\downarrow\uparrow}(\mathbf{k}) + \Gamma_{i,\downarrow\uparrow}(\mathbf{k}')] [\Gamma_{j,\uparrow\downarrow}(\mathbf{k}) + \Gamma_{j,\uparrow\downarrow}(\mathbf{k}')] \\ - [\Gamma_{i,\uparrow\uparrow}(\mathbf{k}) + \Gamma_{i,\uparrow\uparrow}(\mathbf{k}')] [\Gamma_{j,\downarrow\downarrow}(\mathbf{k}) + \Gamma_{j,\downarrow\downarrow}(\mathbf{k}')] . \quad (16)$$

Note that f_{ij} does not depend on the amplitude of \mathbf{k} and \mathbf{k}' , since $\Gamma_{i,\alpha\beta}(\mathbf{k}) + \Gamma_{i,\alpha\beta}(\mathbf{k}') = [(\hat{k} + \hat{k}') \times \sigma_{\alpha\beta}]_i$.

Since $\chi_{ij} = \chi_{ji}$ and $f_{ij} = f_{ji}^*$, it follows that only the real part of f_{ij} contributes to the sum. Using the fact that $|\hat{k} + \hat{k}'|^2 = 2(1 + \hat{k} \cdot \hat{k}')$, the form factor can be re-expressed in the more convenient form:

$$f_{ij}(\hat{k}, \hat{k}') \equiv (1 + \hat{k} \cdot \hat{k}') \delta_{ij} - \frac{1}{2} (\hat{k}_i + \hat{k}'_i) (\hat{k}_j + \hat{k}'_j) \quad (17)$$

Finally, it is convenient to rewrite the bosonic propagator χ_{ij} in terms of its diagonalized form:

$$\chi_{ij}^{-1} = \sum_{a=1,2,3} U_{ia} \tilde{\chi}_{aa}^{-1} U_{aj}^{-1} \quad (18)$$

Here, $\tilde{\chi}_{aa}^{-1} \equiv E_T^{-1} \varpi_a^2$ give the three eigenvalues that correspond to the three phonon dispersions. Furthermore, $U_{ia} \equiv e_a^i$ and $U^{-1} = U^T$, where $\hat{e}_a(\hat{q})$ are the

phonon polarizations. Substituting in Eq. (15) then yields:

$$L(\hat{k}, \hat{k}') = E_T^2 \sum_{a=1,2,3} \frac{\Upsilon_a(\hat{k}, \hat{k}')}{\varpi_a^2(\hat{k} - \hat{k}')} \quad (19)$$

with the modified form factors:

$$\Upsilon_a(\hat{k}, \hat{k}') \equiv \sum_{i,j} U_{ia}(\hat{k} - \hat{k}') f_{ij}(\hat{k}, \hat{k}') U_{aj}^{-1}(\hat{k} - \hat{k}') \quad (20)$$

Related gap equations were derived previously to study the general problem of superconductivity induced by fluctuations of an odd-parity bosonic field [32, 33, 41, 44]. While those works focused on the close competition between even-parity and odd-parity superconducting instabilities, our emphasis here is on the possible application of this formalism to STO, which is believed to be a singlet superconducting state. For this reason, and because the triplet instability was shown to be subleading in the case of the coupling vertex of Eq. (8) [33], in this paper we restrict our analysis to the singlet pairing state only.

III. THE ISOTROPIC SYSTEM

As discussed in the introduction, when the cubic anisotropy term ε_c vanishes in Eq. (1), diagonalization of $\chi_{ij}^{-1}(\mathbf{q}, 0)$ leads to a doubly-degenerate transverse mode, $\varpi_T^2(\mathbf{q}) = \omega_T^2 + E_T^2 q^2$, and a purely longitudinal mode, $\varpi_L^2(\mathbf{q}) = \omega_L^2 + E_L^2 q^2$. To derive the effective pairing interaction $\lambda(\hat{k}, \hat{k}')$ in Eq. (14), we must compute the form factors $\Upsilon_a(\hat{k}, \hat{k}')$ that appear in Eq. (19). In the case of $\varepsilon_c = 0$, it is more convenient to directly invert $\chi_{ij}^{-1}(\mathbf{q}, 0)$, which gives:

$$\frac{\chi_{ij}(\mathbf{q}, 0)}{E_T} = \frac{1}{\varpi_T^2(\mathbf{q})} \left[\delta_{ij} - \left(\frac{\varpi_L^2(\mathbf{q}) - \varpi_T^2(\mathbf{q})}{\varpi_L^2(\mathbf{q})} \right) \hat{q}_i \hat{q}_j \right] \quad (21)$$

We can then directly compute Eq. (15); using the fact that $q^2 = 2k_F^2 (1 - \hat{k} \cdot \hat{k}')$ and $\hat{q}_i = \frac{\hat{k}_i - \hat{k}'_i}{\sqrt{2(1 - \hat{k} \cdot \hat{k}')}}$, we find for the effective pairing interaction:

$$\lambda(x) = \lambda_T(x) + \lambda_L(x) \quad (22)$$

$$\lambda_a(x) = \frac{\lambda_0}{2} \left(\frac{E_T}{\omega_a} \right)^2 \sum_{\pm} \frac{1 \pm x}{1 + 2\eta_a^2(1 \mp x)} \quad (23)$$

where $\eta_a \equiv \frac{E_a k_F}{\omega_a}$ is a dimensionless parameter, $a = T$ or $a = L$, ω_a are the optical gaps of each mode at the zone center, and $x = \hat{k} \cdot \hat{k}' = \cos \theta_{\mathbf{k}, \mathbf{k}'}$ is the relative angle between scattering momenta. Recall that throughout this

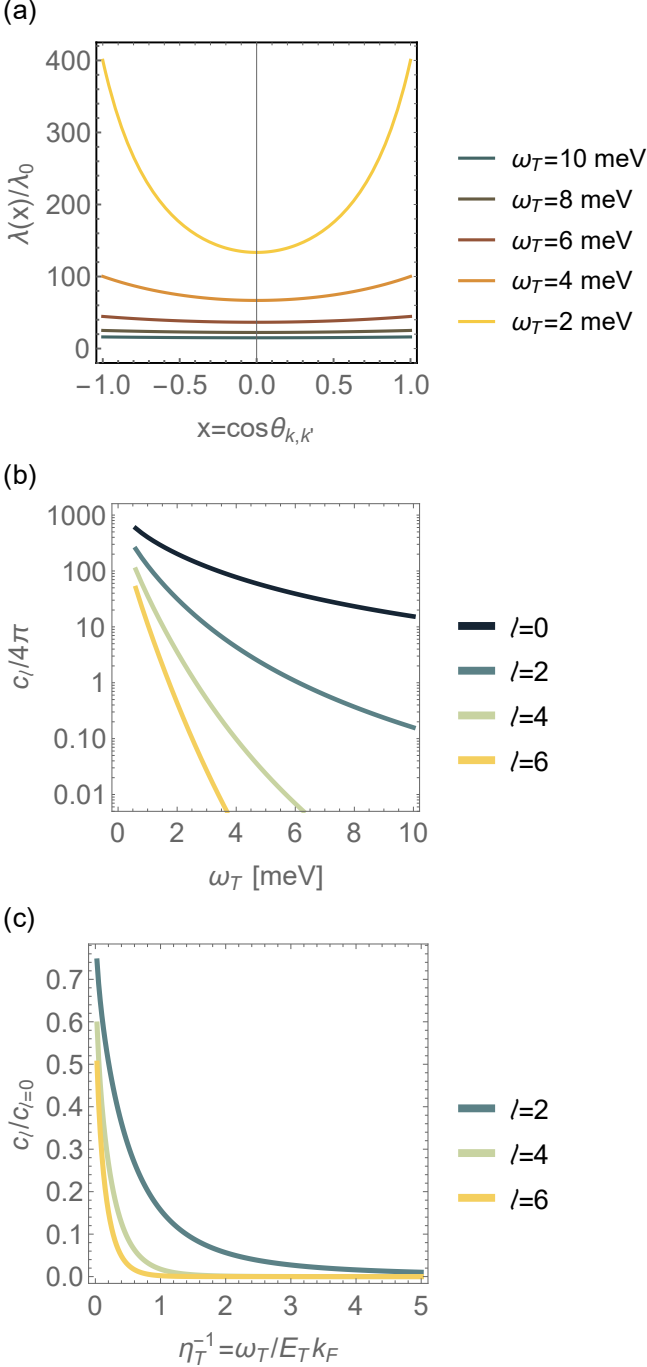


Figure 3. (a) Effective pairing interaction $\lambda(x)$, in units of the dimensionless coupling constant λ_0 , as function of the relative angle between the scattering vectors $x = \cos \theta_{k,k'}$, for different values of the TO mode frequency ω_T . Here, we set $k_F = 0.05$ and $E_T = 40$ meV as relevant for STO, yielding $E_T k_F = 2$ meV. (b) Coefficients c_l of the $l = 0, 2, 4$ and 6 pairing channels as function of ω_T . (c) Ratio between the subdominant coefficients $c_{l>0}$ specified in the legend and the dominant c_0 coefficient as function of the dimensionless parameter $\frac{1}{\eta_T} = \frac{\omega_T}{E_T k_F}$.

work, momentum (and thus k_F) is dimensionless as it is expressed in units of π/a , whereas energies (E_a , ε_c) and frequencies (ω_a) have units of energy.

The pairing interaction $\lambda(x)$ is shown in Fig. 3(a) for several values of the transverse optical gap ω_T . It is positive for all x and thus, in agreement with Ref. [33], it provides an attractive interaction in the even-parity pseudospin-singlet channel. Moreover, because close to the FE instability $\omega_L \gg \omega_T$, the contribution of the longitudinal sector to the pairing interaction $\lambda(x)$ is negligible, $\frac{\lambda_L(x)}{\lambda_T(x)} \sim \left(\frac{\omega_T}{\omega_L}\right)^2 \ll 1$. Consequently, the pairing interaction is mediated primarily through the coupling to the soft transverse mode. This is an important result of our work: in contrast to the dipolar-mediated gradient coupling, the spin-orbit-mediated coupling depends only on the TO mode.

As shown in Fig. 3(a), as the system approaches the FE transition and ω_T decreases, the pairing interaction $\lambda(x)$ increases and becomes more anisotropic, as it depends more strongly on $\theta_{k,k'}$. The maximum of the pairing interaction happens for nearly parallel momenta, $\theta_{k,k'} \approx 0$. This is a direct consequence of the fact that the FE fluctuations are peaked at zero momentum transfer. For $\theta_{k,k'} \approx 0$, $\lambda(x = \pm 1) \approx \lambda_T(x = \pm 1) = \lambda_0 \left(\frac{E_T}{\omega_T}\right)^2$ grows with the softening of the TO mode, whereas for all other angles, the pairing interaction is suppressed by the factor $\eta_T^2 = \left(\frac{E_T k_F}{\omega_T}\right)^2$ in the denominator of Eq. (23). As the TO gap ω_T is reduced and becomes comparable to the characteristic energy $E_T k_F$, the contribution from η_T in the denominator becomes important, and the $\theta_{k,k'}$ anisotropy of the pairing interaction increases, acquiring a pronounced minimum for perpendicular scattering $x = 0$. As will be shown below, this has important consequences for the competition of the various even-parity superconducting channels.

In order to solve the gap equation (13), we exploit the rotational invariance of the system and expand the effective interaction and the gap function into spherical harmonics,

$$\lambda(\hat{k}, \hat{k}') = \lambda_0 \sum_{l,m} c_l Y_l^m(\hat{k}) \left[Y_l^m(\hat{k}') \right]^* \quad (24)$$

$$\Delta(\hat{k}) = \sum_{l,m} d_l Y_l^m(\hat{k}) \quad (25)$$

As a result, the linearized gap equation decouples into orthogonal even-parity channels characterized by the Cooper-pair angular momentum $l = 2n$ ($n \in \mathbb{N}$),

$$1 = \frac{c_l}{4\pi} \lambda_0 \log \left(\frac{1.13 \omega_c}{k_B T_c^{(l)}} \right). \quad (26)$$

The largest coefficient c_l gives the largest superconducting transition temperature $T_c^{(l)}$, thus defining the

leading superconducting instability channel. The coefficients c_l corresponding to the four largest even angular momenta l are shown in Fig. 3(b) as function of the TO mode frequency ω_T . As expected, all coefficients grow for decreasing ω_T , in agreement with the increase of the pairing interaction [Fig. 3(a)]. The $l = 0$ channel has the largest coefficient, signaling an isotropic s -wave gap function at T_c , as expected from an overall attractive pairing interaction $\lambda(x)$. Moreover, as shown in Fig. 3(b), the coefficients of the subleading even-parity channels $l = 2$, $l = 4$ and $l = 6$ grow faster than the isotropic $l = 0$ solution as the system approaches the FE instability, although c_0 always remains larger than $c_{l>0}$ in our calculations.

To understand this behavior, let us focus again on the effective pairing interaction $\lambda(x)$ in Eq. (23). When the frequency of the TO mode is sufficiently large such that $\eta_T = \frac{E_T k_F}{\omega_T} \ll 1$, the interaction is essentially constant, $\lambda(x) \simeq \lambda_0 \frac{E_T^2}{\omega_T^2}$. As a result, $c_0 \gg c_{l>0}$, in analogy to the standard case of a phonon-mediated pairing interaction, which is momentum-independent. Note that this form of the interaction was proposed on phenomenological grounds in Ref. [10]. As the TO mode becomes softer, however, η_T grows and the interaction acquires a strong $\theta_{k,k'}$ anisotropy [Fig. 3(a)], becoming strongly peaked near zero momentum transfer. As a result, the coefficients of the higher-order harmonics increase and approach the isotropic coefficient, $c_{l>0} \rightarrow c_0$, in the regime $\omega_T \ll E_T k_F$, as illustrated in Fig. 3(c). This behavior is reminiscent of the case of pairing mediated by nematic fluctuations, which favor all pairing channels due to the fact that they are also strongly peaked at zero-momentum [45–47].

IV. THE CUBIC SYSTEM

In an actual cubic material, the symmetry is lowered from the continuous rotation group to the discrete point group O_h . In our model, the cubic symmetry of the lattice is manifested by the cubic anisotropy term ε_c in the bosonic propagator (1). In this section, we investigate the impact of this term on the pairing state promoted by the FE fluctuations. Clearly, because ε_c lowers the symmetry of the effective interaction Eq. (15), the superconducting

gap solution $\Delta(\hat{k})$ will no longer be isotropic. As we will show, the anisotropy of the gap generated by this term becomes significant near the FE transition. Note that we neglect, for simplicity, the effect of the cubic crystal field on the electronic band dispersion Eq. (9).

As explained in the introduction and also discussed in Ref. [30], the main effect of the cubic anisotropy on the bosonic degrees of freedom is to couple the polarization of the transverse and longitudinal phonon modes [31]. While the anisotropic term is not small, $\varepsilon_c \sim E_T$ according to fits to neutron data [27], treating ε_c as a perturbation can give powerful insight into the problem. Our strategy in this section is thus to get insight of the gap solution from the perturbative expansion of the pairing interaction in ε_c , and then compare the results with the numerical solution of the gap equation (13).

Treating ε_c as a perturbation, we find that the leading-order correction arising from the polarization of the modes of $\chi_{ij}(\hat{k} - \hat{k}')$ together with the form factor $f_{ij}(\hat{k}, \hat{k}')$ in Eq. (15) vanishes (see Appendix A for details). Thus, the effective pairing interaction is altered solely by the first order correction of the dispersion of the modes. The corresponding expression for the modified interaction Eq. (15) reads,

$$L(\hat{k} - \hat{k}') \simeq \left(\frac{E_T}{\omega_a} \right)^2 \sum_{a=T,L} \frac{1+x}{1+2\eta_a^2(1-x)} \times \left[1 - \frac{\varepsilon_c^2 k_F^2}{2(1-x)\omega_a^2 [1+2\eta_a^2(1-x)]} \zeta_a(\hat{k} - \hat{k}') \right] \quad (27)$$

which is no longer rotational invariant, i.e. it no longer depends only on the relative angle between \hat{k} and \hat{k}' ($x = \cos \hat{k} \cdot \hat{k}'$), but acquires a cubic angular dependence through the form factors ζ_T and ζ_L defined as:

$$\zeta_T(\hat{q}) = 2 (\hat{q}_x^2 \hat{q}_y^2 + \hat{q}_x^2 \hat{q}_z^2 + \hat{q}_y^2 \hat{q}_z^2) \quad (28)$$

$$\zeta_L(\hat{q}) = \hat{q}_x^4 + \hat{q}_y^4 + \hat{q}_z^4. \quad (29)$$

These form factors are plotted in Fig. 4 to highlight their cubic symmetry. The final perturbative expression for the pairing interaction is then $\lambda(\hat{k}, \hat{k}') \simeq \lambda(x) + \lambda_c(\hat{k}, \hat{k}')$, with contributions from the transverse and longitudinal sectors $\lambda_c(\hat{k}, \hat{k}') = \lambda_{c,T}(\hat{k}, \hat{k}') + \lambda_{c,L}(\hat{k}, \hat{k}')$:

$$\lambda_{c,T}(\hat{k}, \hat{k}') = -\frac{\lambda_0}{2} \left(\frac{E_T}{\omega_T} \right)^2 \left(\frac{\varepsilon_c k_F}{\omega_T} \right)^2 \left[\frac{1+x}{1-x} \frac{\sum_{i>j} (\hat{k}_i - \hat{k}'_i)^2 (\hat{k}_j - \hat{k}'_j)^2}{[1+2\eta_T^2(1-x)]^2} + \frac{1-x}{1+x} \frac{\sum_{i>j} (\hat{k}_i + \hat{k}'_i)^2 (\hat{k}_j + \hat{k}'_j)^2}{[1+2\eta_T^2(1+x)]^2} \right] \quad (30)$$

$$\lambda_{c,L}(\hat{k}, \hat{k}') = -\frac{\lambda_0}{4} \left(\frac{E_T}{\omega_L} \right)^2 \left(\frac{\varepsilon_c k_F}{\omega_L} \right)^2 \left[\frac{1+x}{1-x} \frac{\sum_i (\hat{k}_i - \hat{k}'_i)^4}{[1+2\eta_L^2(1-x)]^2} + \frac{1-x}{1+x} \frac{\sum_i (\hat{k}_i + \hat{k}'_i)^4}{[1+2\eta_L^2(1+x)]^2} \right]. \quad (31)$$

The main point of Eqs. (28)-(31) is to illustrate that

the gap function is no longer isotropic, but carries on the

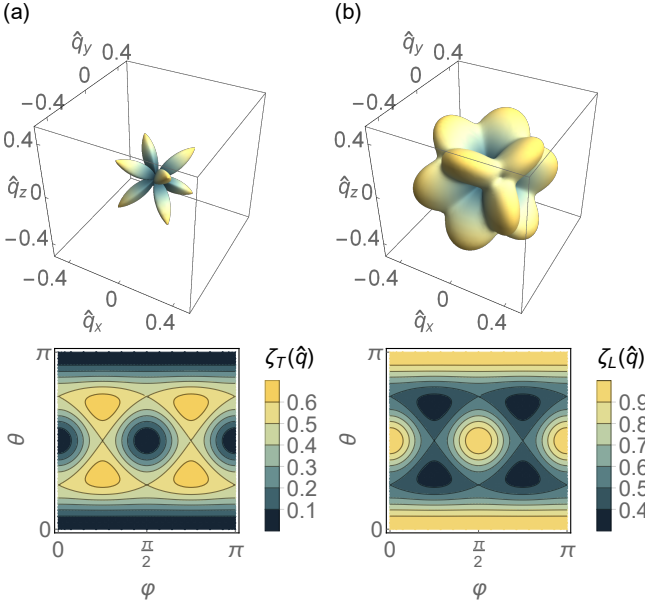


Figure 4. Form factors $\zeta_a(\hat{q})$ obtained in the perturbative treatment of the pairing interaction to leading order in the cubic anisotropy term ε_c . (a) $\zeta_T(\hat{q})$ [Eq. (28)] and (b) $\zeta_L(\hat{q})$ [Eq. (29)]. These form factors enter the effective pairing interaction $L(\hat{q})$ given by Eq. (27).

information encoded in ε_c about the cubic anisotropy of the system. These expression will be used later on to understand qualitatively the results of this section.

In analogy to our solution for the isotropic case, we now have to expand the full pairing interaction (14) (i.e. without assuming small ε_c) into an appropriate set of functions. Instead of spherical harmonics, we use the cubic harmonics $K_a^\Gamma(\hat{k})$ for each irreducible representation (irrep) Γ of the O_h cubic group [48]. For a given irrep, the basis functions $K_a^\Gamma(\hat{k})$ can be expressed in terms of spherical harmonics Y_a^m corresponding to different values of the angular momentum a . The set of basis functions with smallest angular momentum projection a of the five even-parity irreps (A_{1g} , E_g , T_{2g} , T_{1g} and A_{2g}) are shown in Table I. Note that the A_{1g} irrep basis contains functions associated not only with zero angular momentum (“s-wave”), $K_0^{A_{1g}}$, but also with $a = 4$ angular momentum (“g-wave”), $K_4^{A_{1g}}$. This is not surprising, since angular momentum is not a good quantum number for the cubic system.

The full pairing interaction $\lambda(\hat{k}, \hat{k}')$ (and of course the perturbative expressions Eqs. (30)-(31)) mixes, within each irrep Γ , the set of functions $K_a^\Gamma(\hat{k})$. It can therefore be expanded in the following form

$$\lambda(\hat{k}, \hat{k}') = \lambda_0 \sum_{\Gamma} \sum_{ab} c_{ab}^\Gamma K_a^\Gamma(\hat{k}) K_b^\Gamma(\hat{k}') \quad (32)$$

where the coefficients c_{ab} are real numbers. The presence of non-zero $c_{a \neq b}^\Gamma \neq 0$ implies mixing of angular mo-

Table I. Even-parity basis gap-functions of the O_h cubic group for each irreducible representation Γ . Each function is given in terms of real spherical harmonics $Y_l^{m,c}(\hat{k}) \equiv \frac{1}{\sqrt{2}} (Y_l^{-m}(\hat{k}) + Y_l^m(\hat{k}))$ and $Y_l^{m,s}(\hat{k}) \equiv \frac{i}{\sqrt{2}} (Y_l^{-m}(\hat{k}) - Y_l^m(\hat{k}))$. For multi-dimensional irreps, only one of the orthogonal basis is given. From Ref. [48].

Irrep Γ	Representative basis functions
A_{1g}	$K_0^{A_{1g}} = Y_0^0$ $K_4^{A_{1g}}(\hat{k}) = \frac{1}{2} \sqrt{\frac{7}{3}} Y_4^0(\hat{k}) + \frac{1}{2} \sqrt{\frac{5}{3}} Y_4^{4,c}(\hat{k})$
E_g	$K_2^{E_g}(\hat{k}) = Y_2^{2,c}(\hat{k})$ $K_4^{E_g}(\hat{k}) = Y_4^{2,c}(\hat{k})$
T_{2g}	$K_2^{T_{2g}}(\hat{k}) = Y_2^{2,s}(\hat{k})$ $K_4^{T_{2g}}(\hat{k}) = -Y_4^{2,s}(\hat{k})$
T_{1g}	$K_4^{T_{1g}}(\hat{k}) = Y_4^{4,s}(\hat{k})$ $K_6^{T_{1g}}(\hat{k}) = Y_6^{4,s}(\hat{k})$
A_{2g}	$K_6^{A_{2g}}(\hat{k}) = \frac{\sqrt{11}}{4} Y_6^{2,c}(\hat{k}) - \frac{\sqrt{5}}{4} Y_6^{6,c}(\hat{k})$ $K_{10}^{A_{2g}}(\hat{k}) = 0.8 Y_{10}^{2,c}(\hat{k}) + 0.157 Y_{10}^{6,c}(\hat{k}) - 0.576 Y_{10}^{10,c}(\hat{k})$

menta, and therefore the solution of the gap function $\Delta(\hat{k})$ will be in general a combination of cubic harmonics with different angular momenta. We show explicitly in Appendix B that $c_{04}^{A_{1g}} \neq 0$ follows from the perturbative expressions Eqs. (30)-(31).

To proceed, we expand the gap function in cubic harmonics $\Delta(\hat{k}) = \sum_{\Gamma} \sum_a b_a^\Gamma K_a^\Gamma(\hat{k})$. As a result, the superconducting gap equation (13) is decoupled into different irreducible representation channels Γ :

$$\sum_a d_a^\Gamma K_a^\Gamma(\hat{k}) = \lambda_0 \log \left(\frac{1.13 \omega_c}{k_B T_c} \right) \frac{1}{4\pi} \sum_{a,b} d_a^\Gamma c_{ab}^\Gamma K_b^\Gamma(\hat{k}). \quad (33)$$

Our task is then reduced to compute the pairing interaction matrix elements c_{ab}^Γ in Eq. (32), which is numerically straightforward, and then obtain the corresponding largest eigenvalue for each channel Γ . To make the calculations analytically tractable, we truncate the expansion in Eq. (32) into a finite-dimensional matrix in the a, b angular momentum subspace. This is justified as long as the coefficients c_{ab}^Γ decrease with increasing a, b , which we show to be the case below. Note that such a truncation is analogous to the leading angular harmonics approximation (LAHA) method employed to study the gap functions of iron-based superconductors [49].

We focus first on the A_{1g} pairing channel of Eq. (33), corresponding to the trivial irrep of the O_h group. In the previous section, without the cubic anisotropy ($\varepsilon_c = 0$), the leading gap function was found to be the isotropic one, i.e. Y_0^0 (s-wave). Truncating the pairing interaction expansion (32) to second-order gives:

$$\lambda(\hat{k}, \hat{k}') = \lambda_0 \begin{pmatrix} K_0 & K_4(\hat{k}) \end{pmatrix} \begin{pmatrix} c_{00} & c_{04} \\ c_{04} & c_{44} \end{pmatrix} \begin{pmatrix} K_0 \\ K_4(\hat{k}') \end{pmatrix} \quad (34)$$

Here, the $\Gamma = A_{1g}$ superscript has been dropped for

clarity. Solution of the gap equation gives:

$$1 = \lambda_0 \frac{\alpha}{4\pi} \log \left(\frac{1.13\omega_c}{k_B T_c} \right) \quad (35)$$

$$\Delta(\hat{k}) = K_0 + d_4 K_4(\hat{k}), \quad (36)$$

where α is largest eigenvalue of the matrix in Eq. (34) and d_4 can be obtained from the corresponding eigenvector:

$$\alpha = \frac{1}{2} \left(c_{00} + c_{44} + \sqrt{(c_{00} - c_{44})^2 + 4c_{04}^2} \right) \quad (37)$$

$$d_4 = \frac{2c_{04}}{c_{00} - c_{44} + \sqrt{(c_{00} - c_{44})^2 + 4c_{04}^2}}. \quad (38)$$

The A_{1g} gap function $\Delta(\hat{k})$ thus acquires an anisotropic gap structure due to the cubic harmonic K_4 (see Table I). To see why the appearance of this harmonic is generally expected, we rewrite it in Cartesian coordinates:

$$K_4(\hat{k}) = \sqrt{\frac{21}{16\pi}} \left[\hat{k}_x^4 + \hat{k}_y^4 + \hat{k}_z^4 - 3 \left(\hat{k}_x^2 \hat{k}_y^2 + \hat{k}_x^2 \hat{k}_z^2 + \hat{k}_y^2 \hat{k}_z^2 \right) \right] \quad (39)$$

Comparing to the form factors $\zeta_a(\hat{k})$ introduced perturbatively by the cubic anisotropy term ε_c in Eqs. (28) and (29), it is clear that $K_4(\hat{k}) \propto \zeta_L(\hat{k}) - \frac{3}{2}\zeta_T(\hat{k})$. Thus, this form of the gap anisotropy simply reflects the anisotropy in the bosonic propagator.

Fig. 5(a) shows the behavior of the coefficient α as the system approaches the FE instability for various values of the cubic crystal field ε_c . In agreement with what we found in the absence of cubic anisotropy ($\varepsilon_c = 0$, dark blue curve in Fig. 5(a)), the eigenvalue α grows as $\omega_T \rightarrow 0$ for all ε_c values, implying an enhancement of T_c as the FE transition is approached. Moreover, α decreases non-monotonically with the cubic anisotropy ε_c in all the cases we studied (not shown). A larger Fermi momentum k_F also suppresses the eigenvalue α , as seen by comparing Figs. 5(a) and (b), which correspond to $k_F = 0.05$ and $k_F = 0.2$, respectively. Note that the dimensionless electron-FE coupling $\lambda_0 = N_F g^2 / E_T$ may also be enhanced by increasing k_F , particularly if the system starts in the very dilute regime. We do not include this effect in our calculation. Finally, to show that the second-order truncation in Eq. (34) is enough to correctly capture the pairing potential, in Fig. 5(e) we compare the A_{1g} eigenvalue α obtained by truncating at $K_4(\hat{k})$ (filled blue squares) and to next order $K_6(\hat{k})$ (empty yellow squares). Clearly, the correction is very small. Indeed, the coefficient of the next cubic harmonic of the eigenvector $\Delta(\hat{k}) = K_0 + d_4 K_4(\hat{k}) + d_6 K_6(\hat{k})$ is still significantly smaller in this regime of parameter space, i.e. $d_6 \ll d_4$, illustrated in Fig. 5(f).

Fig. 5(c) shows the coefficient d_4 calculated from Eq. (38), which appears in front of the anisotropic contribution $K_4(\hat{k})$ to the gap function, $\Delta(\hat{k}) = K_0 + d_4 K_4(\hat{k})$.

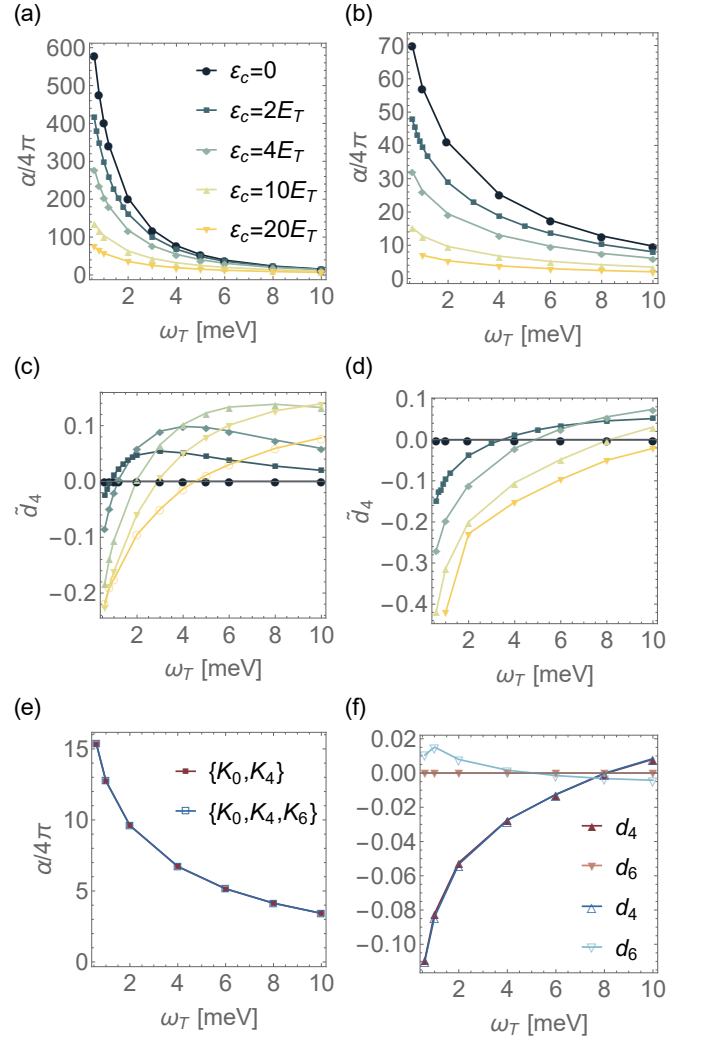


Figure 5. Eigenvalue of the A_{1g} pairing channel α , Eq. (37), for various values of the cubic anisotropy ε_c as specified in the legend, and for (a) $k_F = 0.05$ and (b) $k_F = 0.2$. The corresponding renormalized coefficient \tilde{d}_4 , which is proportional to the anisotropy of the gap function (see definition in the main text), is shown in panels (c) and (d), respectively. (e) Comparison of the computed eigenvalue α for the $\varepsilon_c = 10E_T$ case in panel (b) with $k_F = 0.2$ by including also the next cubic harmonic $K_6(\hat{k})$ in the truncation Eq. (34). (f) Coefficients of the eigenvector $\Delta(\hat{k}) = K_0 + d_4 K_4(\hat{k}) + d_6 K_6(\hat{k})$ of the eigenvalue cases in panel (e).

Since the absolute value of the gap is not fixed by the linearized gap equations, we plot $\tilde{d}_4 = cd_4$, where $c = 3.82$ is the peak-to-peak amplitude of the anisotropic function $K_4(\hat{k})/K_0$, i.e. the difference between the maximum and the minimum of this function. As a result, \tilde{d}_4 gives the relative anisotropy of the gap function. The curves shown in Figs. 5(c)-(d) correspond to the same ε_c values in Figs. 5(a)-(b). As expected, the gap anisotropy \tilde{d}_4 increases with increasing cubic anisotropy ε_c . Interestingly, for a fixed ε_c value, the gap anisotropy shows a

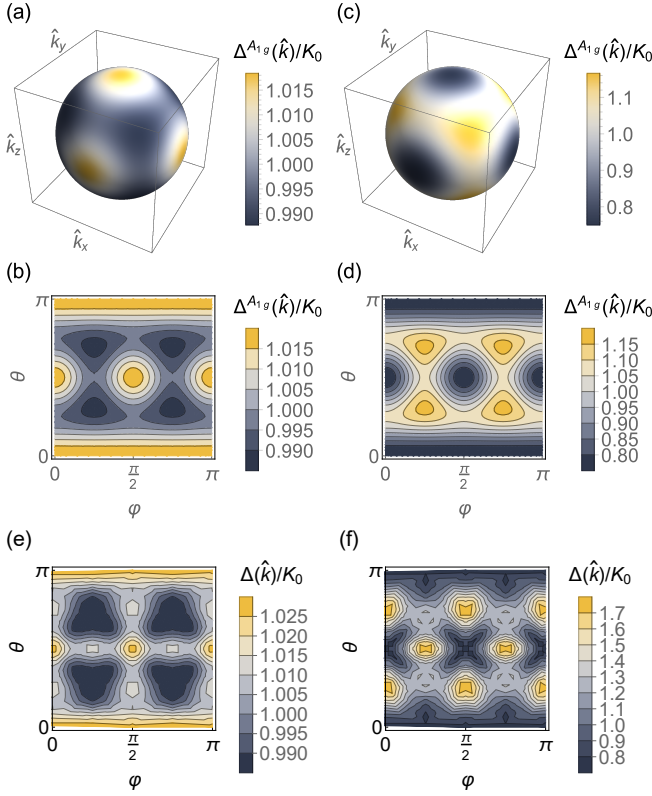


Figure 6. Gap function associated with the A_{1g} pairing instability projected onto the Fermi surface for (a)-(c) $\omega_T = 10$ meV and (d)-(f) $\omega_T = 0.6$ meV. The (a) and (d) ((b) and (e)) panels are three-dimensional (two-dimensional) representations in a sphere (projected on the $\theta - \varphi$ plane). Panels (c) and (f) show the projected gap function of the highest eigenvalue obtained from the direct numerical solution of the gap equation (13). In all panels, $E_T = 40$ meV, $E_L = E_T/10$, $\omega_L = 100$ meV, $\varepsilon_c = 10E_T$ and $k_F = 0.2$.

non-monotonic behavior for decreasing ω_T , even changing sign below a critical value of the TO mode frequency ω_T^* . This critical value depends not only on the cubic anisotropy ε_c , but also on the value of k_F , as it can be seen by comparing panels 5(c) and (d). For the parameters explored here, we find the biggest gap anisotropy to be around 40%, taking place at large cubic anisotropies and small values of the TO gap ω_T .

The full angular dependence of the A_{1g} gap function for $\varepsilon_c = 10E_T$ and $k_F = 0.2$ is shown in Fig. 6 for a large and a small value of ω_T . In Figs. 6(a)-(b), because the TO frequency $\omega_T = 10$ meV is only slightly above the critical value ω_T^* for which d_4 changes sign, the anisotropy of $\Delta(\hat{k})$ is very small. Moreover, because $d_4 > 0$ [see Fig. 5(d)], the gap maxima (light yellow) are located along the $[100]$ and symmetry-related directions, whereas the gap minima (dark blue) appear along the diagonal $[111]$ and symmetry-related directions. For $\omega_T < \omega_T^*$, the gap anisotropy is reversed, since $d_4 < 0$. This is illustrated in Figs. 6(d)-(e), obtained for $\omega_T = 0.6$

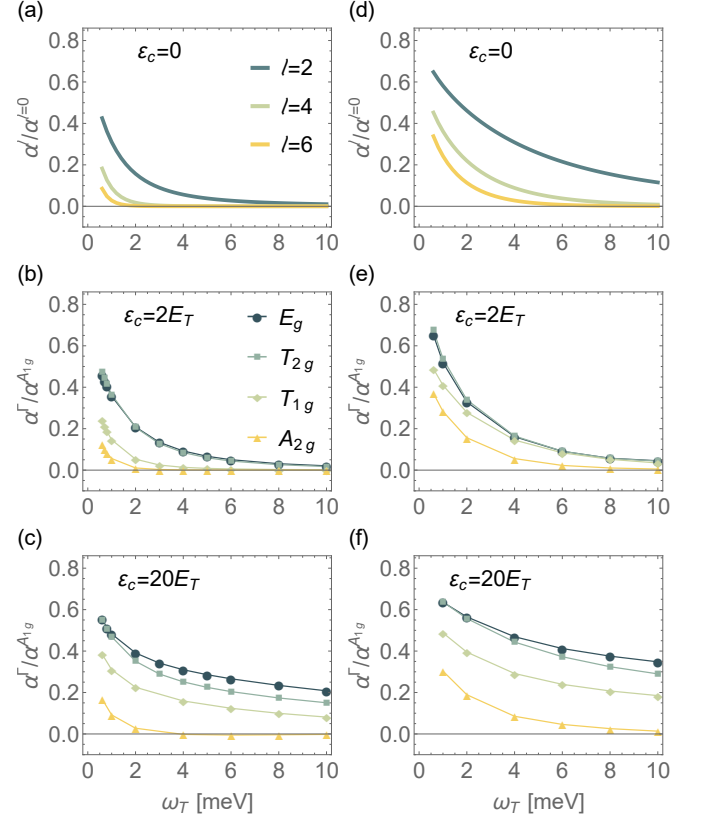


Figure 7. Channel competition for various cubic anisotropy values ε_c as indicated in the insets. (a)-(c) $k_F = 0.05$ and (d)-(f) $k_F = 0.2$.

meV. Besides the switching between the positions of the minima and maxima, we note that the magnitude of the anisotropy is also enhanced, as expected from the enhancement of the magnitude of d_4 upon decreasing ω_T .

In the figures discussed above, we relied on a finite truncation in the expansion of the full interaction Eq. (32). To check whether the conclusions obtained from this method hold, we numerically solved the integral equation Eq. (13) by using a Lebedev quadrature on the sphere [50], an optimized method for cubic numerical integration. As shown in Figs. 6(e)-(f), the numerical gap agrees relatively well with the gap obtained by the truncation method, shown in Fig. 6(b) and Fig. 6(d). This agreement includes the main conclusions that the gap anisotropy changes sign and enhances in magnitude as ω_T decreases. Note that the quantitative agreement is better for larger values of ω_T , indicating that higher-order harmonics become more important as the FE-QCP is approached. This is consistent with what we found in Fig. 5(f).

We now study the pairing instabilities in the other O_h even-parity irreps Γ shown in Table (I). In Fig. 7, we show the leading eigenvalue α^Γ corresponding to each channel (relative to the eigenvalue of the A_{1g} channel) for

different values of the cubic anisotropy ε_c and two different k_F values ($k_F = 0.05$ for the left panels and $k_F = 0.2$ for the right panels). Similarly to the A_{1g} case, we truncate the pairing interaction by considering only the two highest harmonics shown in Table (I) for each irrep. Panels (a) and (d) recover the results discussed in Fig. (3) for the isotropic case, showing that as $\omega_T \rightarrow 0$, higher angular momentum instabilities approach the leading s -wave instability. A similar behavior is seen when the cubic anisotropy is finite, $\varepsilon_c \neq 0$. Indeed, in panels (b)-(c) and (e)-(f), the eigenvalues corresponding to the pairing instabilities in all non-trivial channels become closer to the eigenvalue of the trivial A_{1g} channel as the TO mode becomes softer – although the latter is always larger than the former. Among the non-trivial irreps, the most favored channels are the E_g and T_{2g} ones, usually identified with d -wave pairing. We emphasize however that E_g and T_{2g} also have contributions from $l = 4$ angular momentum (“ g -wave”), as shown in Table (I). The reason for the enhancement of the pairing instabilities in the non-trivial channels seems to be the same for all values of ε_c (including the isotropic case): as $\omega_T \rightarrow 0$, the FE fluctuations become more strongly peaked around $\mathbf{q} = 0$, which tends to favor all pairing states almost equally well.

V. DISCUSSION AND CONCLUSIONS

In this work, we studied the superconducting instability promoted by the exchange of FE fluctuations between low-energy fermions in a cubic system. Focusing on the weak-coupling regime, where the dynamics of the FE fluctuations is not important, we considered the direct coupling between the electronic fermionic operators and the FE bosonic fields mediated by the spin-orbit coupling term (8) [32]. In contrast to the dipolar gradient term arising from the electron-phonon coupling, the main contribution to the pairing interaction comes from the TO soft mode, as the pairing potential becomes proportional to $1/\omega_T^2$. Consequently, we find that T_c is enhanced as the putative FE-QCP is approached, not only in the s -wave singlet channel, but also in all other higher angular momentum even-parity channels, which become closer competitors to the trivial superconducting state.

It is important to emphasize that the general problem of weak-coupling superconductivity caused by the exchange of odd-parity bosonic fluctuations was generally studied in several recent works [32, 33, 41, 42, 44]. In all these works, which considered a variety of different spin-orbit coupling vertices Γ , it was found that odd-parity and even-parity channels are close competitors, and sometimes nearly degenerate. Our work, which considers only the vertex in Eq. (8), reveals in addition that as the bosonic mode becomes soft, all orthogonal even-parity channels become close competitors to the s -wave instability. While here we focused only on the even-parity

states, we expect, based on the results of Ref. [33] for the $l = 1$ channel and for the same vertex Γ , that different odd-parity channels will also be enhanced as $\omega_T \rightarrow 0$. This general phenomenon of multiple nearby pairing instabilities appearing near a putative QCP was also observed in the case of superconductivity mediated by nematic fluctuations [45–47]. Similarly to those, the FE fluctuations considered here also become strongly peaked at $q = 0$ as the QCP is approached. The key point is that $q = 0$ peaked fluctuations, in contrast to the q -independent fluctuations characteristic of the standard electron-phonon interaction, are not effective in coupling states separated by moderate or large momentum transfer. As a result, even though the pairing interaction that they promote is attractive, it does not strongly penalize gap anisotropy.

One of the consequences of the close proximity between the T_c values of different even-parity channels as the FE-QCP is approached, is that certain perturbations may suppress the trivial s -wave state (which always wins in our approach), at the same time that they enhance non- s -wave states – i.e. states with higher Cooper-pair angular momentum. For instance, the onsite Coulomb repulsion will certainly penalize the s -wave state but favor nodal states. Whether this is enough to promote a superconducting transition between two different pairing states as the FE-QCP is approached remains to be investigated. We emphasize that our conclusions rely on a weak-coupling calculation that is valid in a region that excludes the FE-QCP. Although this excluded region can be small if the coupling constant g is small, this approximation prevents us from making statements about the nature of the pairing state at the FE-QCP. At the FE-QCP, the boson dynamics induced by the coupling to the metal’s particle-hole excitations (Landau damping) becomes crucial.

Our main goal here was to apply this type of spin-orbit-mediated coupling between odd-parity bosonic fluctuations and electrons to the case of STO. Experimentally, it is observed that tuning STO towards a putative FE-QCP via Ca doping, strain, or ^{18}O substitution leads to an enhancement of T_c [18–23]. Theoretically, previous works focused either on a phenomenological coupling between the FE soft mode and the electrons [10] or on the microscopic electron-phonon gradient coupling [30, 39, 40]. While the non-soft LO mode plays an important role in the latter case, for the spin-orbit-mediated coupling considered here the pairing interaction is dominated by the soft TO mode. Our work thus provides an interesting alternative avenue by which pairing can be enhanced near the FE-QCP in STO. Of course, there are several features of STO not included in our analysis, such as the role of dilution and the role of the multiple bands that cross the Fermi level as doping is changed [51, 52]. Moreover, the size of the coupling constant g is not known in STO, to the best of our knowledge. As we said above, even if g

is very small, the interaction can still be large as long as the system is close enough to the FE-QCP.

An important property of STO that we included in our analysis is the cubic crystal-field anisotropy of the FE fluctuations, which is not small according to neutron scattering experiments [27]. We find that the main effect of the cubic anisotropy is to induce an anisotropy in the gap function. Although it transforms as the trivial A_{1g} representation of the cubic point group O_h , the gap consists of an admixture of s -wave ($l = 0$) and g -wave ($l = 4$) functions. From this admixture, it follows that the gap displays maxima or minima at high-symmetry directions [100] and [111]. The gap anisotropy changes non-monotonically as ω_T is suppressed, changing sign and enhancing in magnitude as the FE-QCP is approached. Observation of such a gap anisotropy, while challenging, would provide strong experimental support for the relevance of the mechanism discussed here to the understanding of the superconducting state of STO. The best regime to search for such anisotropies would be in the regime of larger doping concentrations, where the Fermi surface is not too small.

While our analysis considered a cubic system, STO is actually tetragonal due to the antiferro-distortive transition it undergoes at about 105 K. Given that the tetragonal distortion is very small with $c/a = 1.00056$ [53], the main results presented here are unlikely to be changed. One interesting consequence of such a small tetragonal distortion is that it couples pairing channels that are otherwise orthogonal in the cubic case. More specifically, the lattice strain $\varepsilon_{zz} = \partial_z u_z$, where \mathbf{u} is the lattice displacement, mixes the A_{1g} and the E_g states. Because the E_g instability becomes a closer competitor to the A_{1g} instability as the FE-QCP is approached, such a mixing could lead to an enhancement of T_c [54].

Beyond STO, our work should be relevant for other metallic systems in which ferroelectric fluctuations are strong and superconductivity is nearby. A recent work focused on the case of Dirac electrons coupled to FE fluctuations [42]. The boson-fermion coupling term considered in that work is analogous to the one studied here, with valley degrees of freedom playing the role of spin degrees of freedom. Interestingly, Ref. [42] did find a strong enhancement of T_c near the FE-QCP. One could also conceive heterostructures with substrates that can be continuously tuned across a FE transition, e.g. ATiO_3 with cation A . If a very thin metallic film is deposited on top of such a substrate, the FE fluctuations of the latter may provide an additional source of pairing in the metal. Since the FE fluctuations favor a variety of different pairing channels, an enhancement of T_c would be expected.

We thank A. Balatsky, K. Behnia, A. Chubukov, A. Klein, V. Kozii, G. Lonzarich, J. Ruhman, and P. Woelfle for insightful discussions. MNG and RMF were supported by the U. S. Department of Energy through the

University of Minnesota Center for Quantum Materials, under Award No. DE-SC-0016371. TVT was supported by São Paulo Research Foundation (Fapesp, Brazil) via fellowship 2015/21349-7.

Appendix A: Perturbative calculation of the interaction due to the cubic anisotropy term ε_c

In this section we explicitly derive Eq. (27), the expression of the coupling function $L(\hat{k}, \hat{k}')$ [Eq. (15)] when treating the cubic crystal field term ε_c perturbatively. We start with the rotationally invariant case $\varepsilon_c = 0$ explored in Section III. The phonon dispersions acquire the simple expressions $\varpi_a^2(q) = \omega_a^2 + E_a^2 q^2$ for the two-fold degenerate transverse mode ($a = T$) and the longitudinal mode ($a = L$), with polarizations

$$\hat{e}_{T1}(\hat{q}) = A(\hat{q}) (-\hat{q}_z, 0, \hat{q}_x) \quad (\text{A1})$$

$$+ B(\hat{q}) (-\hat{q}_y |\hat{q}_x|, (\hat{q}_x^2 + \hat{q}_z^2) \text{sgn}(\hat{q}_x), -\hat{q}_y \hat{q}_z \text{sgn}(\hat{q}_x))$$

$$\hat{e}_{T2}(\hat{q}) = C(\hat{q}) (-\hat{q}_z, 0, \hat{q}_x) \quad (\text{A2})$$

$$+ D(\hat{q}) (-\hat{q}_y |\hat{q}_x|, (\hat{q}_x^2 + \hat{q}_z^2) \text{sgn}(\hat{q}_x), -\hat{q}_y \hat{q}_z \text{sgn}(\hat{q}_x))$$

$$\hat{e}_L(\hat{q}) = (\hat{q}_x, \hat{q}_y, \hat{q}_z) \quad (\text{A3})$$

where the coefficients in the transverse subspace $A(\hat{q})$, $B(\hat{q})$, $C(\hat{q})$ and $D(\hat{q})$ are chosen to keep the basis $\{\hat{e}_a(\hat{q})\}$ orthonormal. The expression of the rotationally invariant coupling function is then

$$L(x) = \sum_{a=L,T} \frac{E_T^2}{\omega_a^2} \frac{1+x}{1+2\eta_a^2(1+x)} \quad (\text{A4})$$

which gives the isotropic kernel $\lambda(x) = \frac{\lambda_0}{2} (L(x) + L(-x))$ in Eq. (23).

We now introduce the cubic anisotropy term:

$$\varepsilon_c^2 q^2 \hat{q}_i \delta_{ij} \equiv \varepsilon_c^2 q^2 W_{ij}(\hat{q}) \quad (\text{A5})$$

perturbatively in the bosonic propagator Eq. (1), and calculate how the coupling function $L(x)$ is modified through the changes in the eigenmodes of the propagator. Since in the absence of the perturbation the transverse subspace [Eqs. (A1)-(A2)] is doubly degenerate, in order to apply perturbation theory we first choose the set of coefficients $A(\hat{q})$, $B(\hat{q})$, $C(\hat{q})$ and $D(\hat{q})$ so that the off-diagonal matrix element of the cubic anisotropy perturbative term vanishes, i.e., $\langle \hat{e}_{T1}(\hat{q}) | W | \hat{e}_{T2}(\hat{q}) \rangle = 0$. We can now proceed to calculate the modification of the eigenmodes. First, the perturbation term W lifts the degeneracy of the transverse modes with modified dispersions $\varpi_a'^2(\hat{q}) \simeq \varpi_a^2(q) + \varepsilon_c^2 q^2 \zeta_a(\hat{q})$ up to order $\mathcal{O}(\varepsilon_c^2 q^2)$

where

$$\zeta_{T1}(\hat{q}) = \hat{q}_x^2 \hat{q}_y^2 + \hat{q}_x^2 \hat{q}_z^2 + \hat{q}_y^2 \hat{q}_z^2 - \sqrt{\hat{q}_x^4 \hat{q}_y^4 + \hat{q}_x^4 \hat{q}_z^4 + \hat{q}_y^4 \hat{q}_z^4 - \hat{q}_x^2 \hat{q}_y^2 \hat{q}_z^2} \quad (\text{A6})$$

$$\zeta_{T2}(\hat{q}) = \hat{q}_x^2 \hat{q}_y^2 + \hat{q}_x^2 \hat{q}_z^2 + \hat{q}_y^2 \hat{q}_z^2 + \sqrt{\hat{q}_x^4 \hat{q}_y^4 + \hat{q}_x^4 \hat{q}_z^4 + \hat{q}_y^4 \hat{q}_z^4 - \hat{q}_x^2 \hat{q}_y^2 \hat{q}_z^2} \quad (\text{A7})$$

$$\zeta_L(\hat{q}) = \hat{q}_x^4 + \hat{q}_y^4 + \hat{q}_z^4. \quad (\text{A8})$$

The eigenvectors $\hat{e}_a(\hat{q})$ in Eqs. (A1)-(A3) are also modified by the perturbation term W with $\hat{e}'_a(\hat{q}) \simeq \hat{e}_a(\hat{q}) + \varepsilon_c^2 q^2 u_a(\hat{q})$:

$$u_{T1}(\hat{q}) = -\frac{W_{T1,L}(\hat{q})\hat{e}_L(\hat{q})}{\varpi_L^2(q) - \varpi_T^2(q)} \quad (\text{A9})$$

$$u_{T2}(\hat{q}) = -\frac{W_{T2,L}(\hat{q})\hat{e}_L(\hat{q})}{\varpi_L^2(q) - \varpi_T^2(q)} \quad (\text{A10})$$

$$u_L(\hat{q}) = \frac{W_{T1,L}(\hat{q})\hat{e}_{T1}(\hat{q}) + W_{T2,L}(\hat{q})\hat{e}_{T2}(\hat{q})}{\varpi_L^2(q) - \varpi_T^2(q)} \quad (\text{A11})$$

Here, we defined the notation $W_{a,b}(\hat{q}) = \langle \hat{e}_a | W | \hat{e}_b \rangle$ for the perturbation matrix elements. We can thus calculate the correction of the numerator in the coupling function Eq. (19), $\Upsilon'_a(\hat{q}) \simeq \Upsilon_a(q) + \varepsilon_c^2 q^2 \Phi_a(\hat{q})$ with

$$\Phi_{T1}(\hat{k}, \hat{k}') = -\frac{2W_{T1,L}(\hat{q})}{\varpi_L^2(q) - \varpi_T^2(q)} \times \quad (\text{A12})$$

$$\sum_{i,j=x,y,z} u_{L,i}(\hat{q}) u_{T1,j}(\hat{q}) (\hat{k}_i + \hat{k}'_i) (\hat{k}_j + \hat{k}'_j)$$

$$\Phi_{T2}(\hat{k}, \hat{k}') = -\frac{2W_{T2,L}(\hat{q})}{\varpi_L^2(q) - \varpi_T^2(q)} \times \quad (\text{A13})$$

$$\sum_{i,j=x,y,z} u_{L,i}(\hat{q}) u_{T2,j}(\hat{q}) (\hat{k}_i + \hat{k}'_i) (\hat{k}_j + \hat{k}'_j)$$

$$\Phi_L(\hat{k}, \hat{k}') = -\left[\Phi_{T1}(\hat{k}, \hat{k}') + \Phi_{T2}(\hat{k}, \hat{k}') \right], \quad (\text{A14})$$

and $\hat{q} = (\hat{k} - \hat{k}') / \sqrt{2(1 - \hat{k} \cdot \hat{k}')}.$ Because of the form of the longitudinal polarization $\hat{e}_L(\hat{q})$ [Eq. (A3)], the following equality is fulfilled,

$$\sum_{i=x,y,z} u_{L,i}(\hat{q}) u_{a,i}(\hat{q}) (\hat{k}_i + \hat{k}'_i)^2 = -\sum_{i \neq j} u_{L,i}(\hat{q}) u_{a,j}(\hat{q}) (\hat{k}_i + \hat{k}'_i) (\hat{k}_j + \hat{k}'_j) \longrightarrow \Phi_a(\hat{q}) = 0. \quad (\text{A15})$$

Therefore, the leading order correction of $\Upsilon_a(\hat{q})$ vanishes and, as mentioned in the main text, only the correction to the eigenvalues $\varpi'_a(\hat{q})$ contributes in this order to the modified expression of the pairing interaction, given by Eq. (27).

Appendix B: Non-zero c_{04}^{A1g} mixing term

We focus on the simplest limit of the lengthy expressions Eqs. (30)-(31): $\omega_a^2 \ll E_a^2 k_F^2$, so we can take $\eta_a^2 \approx 0$

in the denominators of both expressions (note that for the massive longitudinal mode this is a very good approach, but for the soft transverse mode it is just one of the possible limits that depend on the ratio $\frac{\omega_T}{E_T k_F}$). For simplicity, we also set $x = 0$, which we can do without loss of generality in order to show that $c_{40}^{A1g} \neq 0$. The sign of c_{40} , however, depends on the contribution of all x . Under these approximations the expressions become:

$$\lambda_{c,T}(\hat{k}, \hat{k}') \simeq -\lambda_0 \left(\frac{E_T}{\omega_T} \right)^2 \left(\frac{\varepsilon_c k_F}{\omega_T} \right)^2 \left[\hat{k}_x^2 \hat{k}_y^2 + \hat{k}_x^2 \hat{k}_z^2 + \hat{k}_y^2 \hat{k}_z^2 + \hat{k}_x'^2 \hat{k}_y'^2 + \hat{k}_x'^2 \hat{k}_z'^2 + \hat{k}_y'^2 \hat{k}_z'^2 + 1 - 3 \left(\hat{k}_x^2 \hat{k}_x'^2 + \hat{k}_y^2 \hat{k}_y'^2 + \hat{k}_z^2 \hat{k}_z'^2 \right) \right] \quad (\text{B1})$$

$$\lambda_{c,L}(\hat{k}, \hat{k}') \simeq -\frac{\lambda_0}{2} \left(\frac{E_T}{\omega_L} \right)^2 \left(\frac{\varepsilon_c k_F}{\omega_L} \right)^2 \left[\hat{k}_x^4 + \hat{k}_y^4 + \hat{k}_z^4 + \hat{k}_x'^4 + \hat{k}_y'^4 + \hat{k}_z'^4 + 6 \left(\hat{k}_x^2 \hat{k}_x'^2 + \hat{k}_y^2 \hat{k}_y'^2 + \hat{k}_z^2 \hat{k}_z'^2 \right) \right]. \quad (\text{B2})$$

Comparing Eqs.(B1) and (B2) with Eq. (39), we im-

mediately see their similarities with the cubic harmonics. More concretely we can rewrite the expressions as

$$\lambda_{c,T}(\hat{k}, \hat{k}') \propto -\frac{1}{2} \sum_{i>j} [(\hat{k}_i - \hat{k}'_i)^2 (\hat{k}_j - \hat{k}'_j)^2 + (\hat{k}_i + \hat{k}'_i)^2 (\hat{k}_j + \hat{k}'_j)^2] \approx \frac{8\pi}{5} \begin{pmatrix} K_0^{A_{1g}} & K_4^{A_{1g}}(\hat{k}) \end{pmatrix} \begin{pmatrix} -\frac{8}{3} & \frac{1}{\sqrt{21}} \\ \frac{1}{\sqrt{21}} & 0 \end{pmatrix} \begin{pmatrix} K_0^{A_{1g}} \\ K_4^{A_{1g}}(\hat{k}') \end{pmatrix} \quad (\text{B3})$$

$$\lambda_{c,L}(\hat{k}, \hat{k}') \propto -\frac{1}{4} \sum_i [(\hat{k}_i - \hat{k}'_i)^4 + (\hat{k}_i + \hat{k}'_i)^4] \approx \frac{8\pi}{5} \begin{pmatrix} K_0^{A_{1g}} & K_4^{A_{1g}}(\hat{k}) \end{pmatrix} \begin{pmatrix} -4 & -\frac{1}{\sqrt{21}} \\ -\frac{1}{\sqrt{21}} & 0 \end{pmatrix} \begin{pmatrix} K_0^{A_{1g}} \\ K_4^{A_{1g}}(\hat{k}') \end{pmatrix}, \quad (\text{B4})$$

where we truncated the expansions in cubic harmonics to leading order. Note that in both cases, the angular momentum mixing coefficient $c_{40}^{A_{1g}} \neq 0$.

* Present address: ISC-CNR and Department of Physics, Sapienza University of Rome, Piazzale Aldo Moro 2, I-00185, Rome, Italy.

† Present address: Ames Laboratory, Ames, Iowa 50011, USA

-
- [1] P. Monthoux, A. V. Balatsky, and D. Pines, *Phys. Rev. Lett.* **67**, 3448 (1991).
 - [2] A. Abanov, A. V. Chubukov, and J. Schmalian, *Advances in Physics* **52**, 119 (2003).
 - [3] D. J. Scalapino, *Rev. Mod. Phys.* **84**, 1383 (2012).
 - [4] L. Taillefer, *Annu. Rev. Condens. Matter Phys.* **1**, 51 (2010).
 - [5] M. A. Metlitski and S. Sachdev, *Phys. Rev. B* **82**, 075128 (2010).
 - [6] X. Wang, Y. Schattner, E. Berg, and R. M. Fernandes, *Phys. Rev. B* **95**, 174520 (2017).
 - [7] R. Roussev and A. J. Millis, *Phys. Rev. B* **63**, 140504 (2001).
 - [8] M. A. Metlitski, D. F. Mross, S. Sachdev, and T. Senthil, *Phys. Rev. B* **91**, 115111 (2015).
 - [9] S. Lederer, Y. Schattner, E. Berg, and S. A. Kivelson, *Proceedings of the National Academy of Sciences* **114**, 4905 (2017).
 - [10] J. M. Edge, Y. Kedem, U. Aschauer, N. A. Spaldin, and A. V. Balatsky, *Phys. Rev. Lett.* **115**, 247002 (2015).
 - [11] P. Chandra, G. G. Lonzarich, S. Rowley, and J. Scott, *Reports on Progress in Physics* **80**, 112502 (2017).
 - [12] M. N. Gastiasoro, J. Ruhman, and R. M. Fernandes, *arXiv preprint arXiv:1912.01509* (2019).
 - [13] K. A. Müller and H. Burkard, *Phys. Rev. B* **19**, 3593 (1979).
 - [14] S. Rowley, L. Spalek, R. Smith, M. Dean, M. Itoh, J. Scott, G. Lonzarich, and S. Saxena, *Nature Physics* **10**, 367 (2014).
 - [15] C. S. Koonce, M. L. Cohen, J. F. Schooley, W. R. Hosler, and E. R. Pfeiffer, *Phys. Rev.* **163**, 380 (1967).
 - [16] X. Lin, G. Bridoux, A. Gourgout, G. Seyfarth, S. Krämer, M. Nardone, B. Fauqué, and K. Behnia, *Phys. Rev. Lett.* **112**, 207002 (2014).
 - [17] T. M. Bretz-Sullivan, A. Edelman, J. Jiang, A. Suslov, D. Graf, J. Zhang, G. Wang, C. Chang, J. E. Pearson, A. B. Martinson, *et al.*, *arXiv preprint arXiv:1904.03121* (2019).
 - [18] A. Stucky, G. Scheerer, Z. Ren, D. Jaccard, J.-M. Pouchard, C. Barreteau, E. Giannini, and D. van der Marel, *Scientific reports* **6**, 37582 (2016).
 - [19] C. W. Rischau, X. Lin, C. P. Grams, D. Finck, S. Harms, J. Engelmayer, T. Lorenz, Y. Gallais, B. Fauqué, J. Hemberger, *et al.*, *Nature Physics* **13**, 643 (2017).
 - [20] Y. Tomioka, N. Shirakawa, K. Shibuya, and I. H. Inoue, *Nature communications* **10**, 738 (2019).
 - [21] S. Rowley, C. Enderlein, J. F. de Oliveira, D. Tompsett, E. B. Saitovitch, S. Saxena, and G. Lonzarich, *arXiv preprint arXiv:1801.08121* (2018).
 - [22] C. Herrera, J. Cerbin, A. Jayakody, K. Dunnett, A. V. Balatsky, and I. Sochnikov, *Phys. Rev. Materials* **3**, 124801 (2019).
 - [23] R. Russell, N. Ratcliff, K. Ahadi, L. Dong, S. Stemmer, and J. W. Harter, *Phys. Rev. Materials* **3**, 091401 (2019).
 - [24] H. Weaver, *Journal of Physics and Chemistry of Solids* **11**, 274 (1959).
 - [25] W. Cochran, *Advances in Physics* **9**, 387 (1960).
 - [26] R. A. Cowley, *Phys. Rev.* **134**, A981 (1964).
 - [27] Y. Yamada and G. Shirane, *Journal of the Physical Society of Japan* **26**, 396 (1969).
 - [28] J. Scott, *Reviews of Modern Physics* **46**, 83 (1974).
 - [29] Y. Shi, Y. Guo, X. Wang, A. J. Princep, D. Khalyavin, P. Manuel, Y. Michiue, A. Sato, K. Tsuda, S. Yu, *et al.*, *Nature materials* **12**, 1024 (2013).
 - [30] P. Wölffe and A. V. Balatsky, *Phys. Rev. B* **98**, 104505 (2018).
 - [31] J. Ruhman and P. A. Lee, *Phys. Rev. B* **100**, 226501 (2019).
 - [32] L. Fu, *Phys. Rev. Lett.* **115**, 026401 (2015).
 - [33] V. Kozii and L. Fu, *Phys. Rev. Lett.* **115**, 207002 (2015).
 - [34] S. Kanasugi and Y. Yanase, *Phys. Rev. B* **98**, 024521 (2018).
 - [35] S. Kanasugi and Y. Yanase, *Phys. Rev. B* **100**, 094504 (2019).
 - [36] M. N. Gastiasoro, A. V. Chubukov, and R. M. Fernandes, *Phys. Rev. B* **99**, 094524 (2019).
 - [37] R. Roussev and A. J. Millis, *Phys. Rev. B* **67**, 014105 (2003).
 - [38] G. J. Conduit and B. D. Simons, *Phys. Rev. B* **81**, 024102 (2010).
 - [39] J. R. Arce-Gamboa and G. G. Guzmán-Verri, *Phys. Rev. Materials* **2**, 104804 (2018).
 - [40] Y. Kedem, *Phys. Rev. B* **98**, 220505 (2018).
 - [41] F. Wu and I. Martin, *Phys. Rev. B* **96**, 144504 (2017).
 - [42] V. Kozii, Z. Bi, and J. Ruhman, *Phys. Rev. X* **9**, 031046 (2019).
 - [43] J. Ruhman and P. A. Lee, *Phys. Rev. B* **94**, 224515 (2016).
 - [44] P. M. R. Brydon, S. Das Sarma, H.-Y. Hui, and J. D.

- Sau, Phys. Rev. B **90**, 184512 (2014).
- [45] S. Lederer, Y. Schattner, E. Berg, and S. A. Kivelson, Phys. Rev. Lett. **114**, 097001 (2015).
 - [46] J. Kang and R. M. Fernandes, Phys. Rev. Lett. **117**, 217003 (2016).
 - [47] A. Klein, Y.-M. Wu, and A. Chubukov, arXiv preprint arXiv:1812.00521 (2018).
 - [48] S. L. Altmann and A. P. Cracknell, Rev. Mod. Phys. **37**, 19 (1965).
 - [49] S. Maiti, M. M. Korshunov, T. A. Maier, P. J. Hirschfeld, and A. V. Chubukov, Phys. Rev. B **84**, 224505 (2011).
 - [50] V. I. Lebedev, USSR Computational Mathematics and Mathematical Physics **16**, 10 (1976).
 - [51] T. V. Trevisan, M. Schütt, and R. M. Fernandes, Phys. Rev. Lett. **121**, 127002 (2018).
 - [52] T. V. Trevisan, M. Schütt, and R. M. Fernandes, Phys. Rev. B **98**, 094514 (2018).
 - [53] F. W. Lytle, Journal of Applied Physics **35**, 2212 (1964).
 - [54] J. Kang, A. F. Kemper, and R. M. Fernandes, Phys. Rev. Lett. **113**, 217001 (2014).